Supplementary Material: Deriving seasonal and annual surface mass balance for debris-covered glaciers from flow-corrected satellite stereo DEM time series

Shashank Bhushan[1], David Shean[1], J. Michelle Hu[1], Grégoire Guillet[1], David R. Rounce[2]

[1]*Department of Civil & Environmental Engineering, University of Washington, WA, USA*

[2]*Department of Civil & Environmental Engineering, Carnegie Mellon University, PA, USA*

Correspondence: Shashank Bhushan <sbaglapl@uw.edu>

S1 INTRODUCTION

This document contains additional supplementary tables (Table S1 - S4) and figures (Figures S1 - S8) supporting the content in the main manuscript.

S2 SUPPLEMENTARY TABLES

Table S1. List of Maxar stereo images used in this study. All dates are in YYYYMMDD format.

Glacier	Acquisition Date	Sensor	Catalog ID 1	Catalog ID 2	Finest Pan GSD (m)
Imja Lhotse Shar	20151002	WV01	10200100457F0C00	1020010042C0CE00	0.51
	20161029	WV02	103001005E3EFF00	103001005E3A0D00	0.53
Khumbu	20151102	WV03	10400100130D8500	10400100125E8E00	0.35
	20161025	WV03	1040010024438E00	104001002469AD00	0.34
Black Changri Nup	20151102[a]	WV03	10400100130D8500	10400100125E8E00	0.35
	20160422[a]	WV02	103001005401B300	103001005444C600	0.50
	20161025[a]	WV03	1040010024438E00	104001002469AD00	0.34
Ngozumpa	20121223	GE01	1050410000E8C900	1050410000E0AE00	0.42
	20150115	WV03	1040010006A12900	104001000665F400	0.31
Langtang	20150222	WV03	1040010008B92D00	10400100087E2400	0.32
	20160107	WV02	103001004F89CB00	103001004E783B00	0.55
Lirung	20150122[a]	WV03	1040010006841E00	10400100060FE200	0.35
	20150508[a]	WV03	104001000BA62E00	104001000B3B2300	0.37
	20151229[a]	WV01	1020010046506C00	10200100496BE700	0.54
	20161106	WV02	103001005F7EBB00	103001005FAB7A00	0.52
	20171222	WV01	102001006F214E00	10200100688AC000	0.53

[a]Observations used for seasonal analysis.

Table S2. Mean expected elevation change due to slope-parallel flow ($\boldsymbol{u_s} \cdot \nabla h$) and flux divergence (f$\nabla \cdot (H\boldsymbol{u_s})$) before and after application of the thickness-dependent Gaussian filter. Units are m/yr.

Glacier Name	pre-filter $\boldsymbol{u_s} \cdot \nabla h$	post-filter $\boldsymbol{u_s} \cdot \nabla h$	pre-filter f$\nabla \cdot (H\boldsymbol{u_s})$	post-filter f$\nabla \cdot (H\boldsymbol{u_s})$
Imja Lhotse Shar	-0.65	-0.59	-0.32	-0.29
Khumbu	-1.00	-0.97	-0.67	-0.62
Black Changri Nup	-1.17	-1.17	-0.02	-0.02
Ngozumpa	-0.74	-0.73	-0.39	-0.35
Langtang	-1.30	-1.30	-0.18	-0.19
Lirung	-0.34	-0.35	-0.16	-0.12

Table S3. Mean Eulerian elevation change rate ($\frac{dh}{dt}$) and slope-corrected Lagrangian elevation change rate ($\frac{Dh}{Dt} - \boldsymbol{u_s}\nabla h$) over all valid pixels for each glacier. Units are m/yr.

Glacier Name	$\frac{dh}{dt}$	$\frac{Dh}{Dt} - \boldsymbol{u_s}\nabla h$
Imja Lhotse Shar	-0.86	-0.90
Khumbu	-1.01	-1.10
Black Changri Nup	-0.58	-0.59
Ngozumpa	-0.99	-1.01
Langtang	-1.17	-1.18
Lirung	-2.01	-2.05

Table S4. Observed systematic and random error of surface velocity ($\boldsymbol{u_s}$) and slope-corrected Lagrangian elevation change rate ($\frac{Dh}{Dt} - \boldsymbol{u_s}\nabla h$) products over non-glacierized, static surfaces surrounding each glacier. The combined root sum of the two squared error estimates is used to estimate corresponding uncertainty of these products over glacier surfaces. Units are m/yr.

Glacier Name	$\boldsymbol{u_s}$			$\frac{Dh}{Dt} - \boldsymbol{u_s}\nabla h$		
	med	NMAD	combined	med	NMAD	combined
Imja Lhotse Shar	0.79	0.42	0.89	0.14	0.55	0.57
Khumbu	0.58	0.31	0.66	0.02	0.45	0.45
Black Changri Nup	0.68	0.35	0.76	-0.01	0.50	0.50
Ngozumpa	0.51	0.17	0.54	-0.05	0.30	0.30
Langtang	1.48	0.60	1.60	-0.03	1.03	1.03
Lirung	0.85	0.41	0.94	0.10	0.42	0.43

S3 SUPPLEMENTARY FIGURES

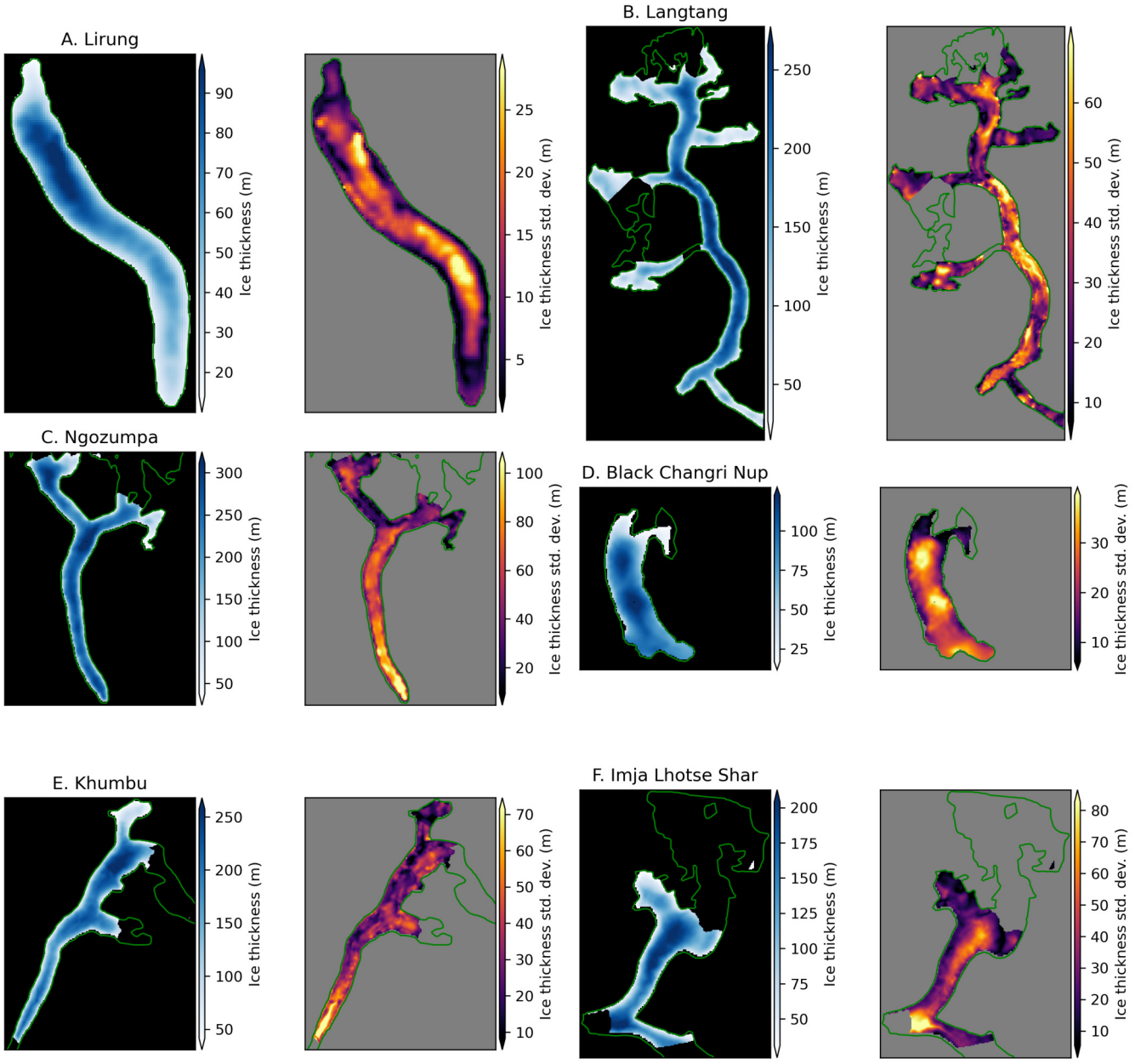

Fig. S1. Consensus ice thickness map (H) of Farinotti and others (2019), and weighted ice thickness standard deviation map (σ_H) computed from the four available input ice thickness models, M1: (Huss and Farinotti, 2012), M2: (Frey and others, 2014), M3: (Maussion and others, 2019), M4: (Fürst and others, 2017).

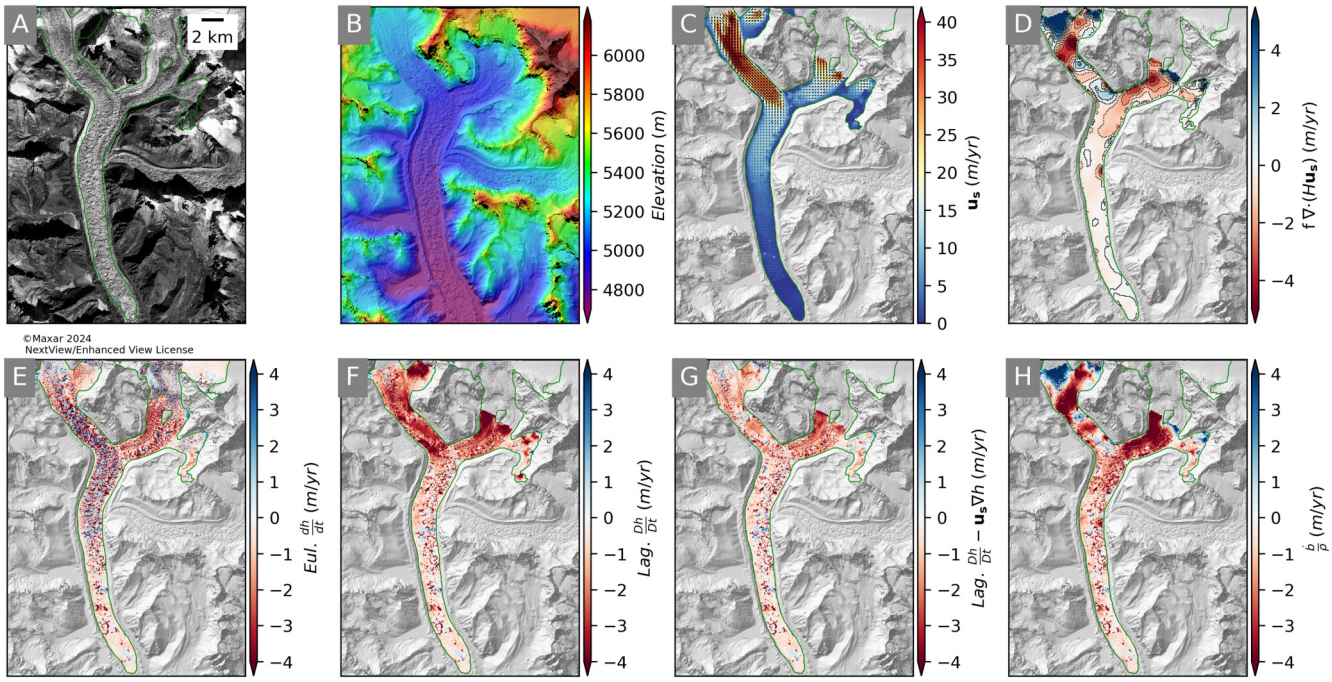

Fig. S2. Subset of data products over Ngozumpa Glacier for the period 23 December 2012 to 15 January 2015: A) Panchromatic GE01 orthoimage from 23 December 2012, B) Color shaded relief map, C) Surface velocity ($\boldsymbol{u_s}$), D) Flux divergence (f$\nabla \cdot (H\boldsymbol{u_s})$) with 1 meter contours, E) Eulerian elevation change rate ($\frac{dh}{dt}$), F) Lagrangian elevation change rate ($\frac{Dh}{Dt}$), G) Slope-corrected Lagrangian elevation change rate ($\frac{Dh}{Dt} - \boldsymbol{u_s}\nabla h$), and H) Lagrangian SMB rate ($\frac{\dot{b}}{\rho}$) obtained by adding flux divergence (panel D) to the Slope-corrected Lagrangian elevation change rate (panel G).

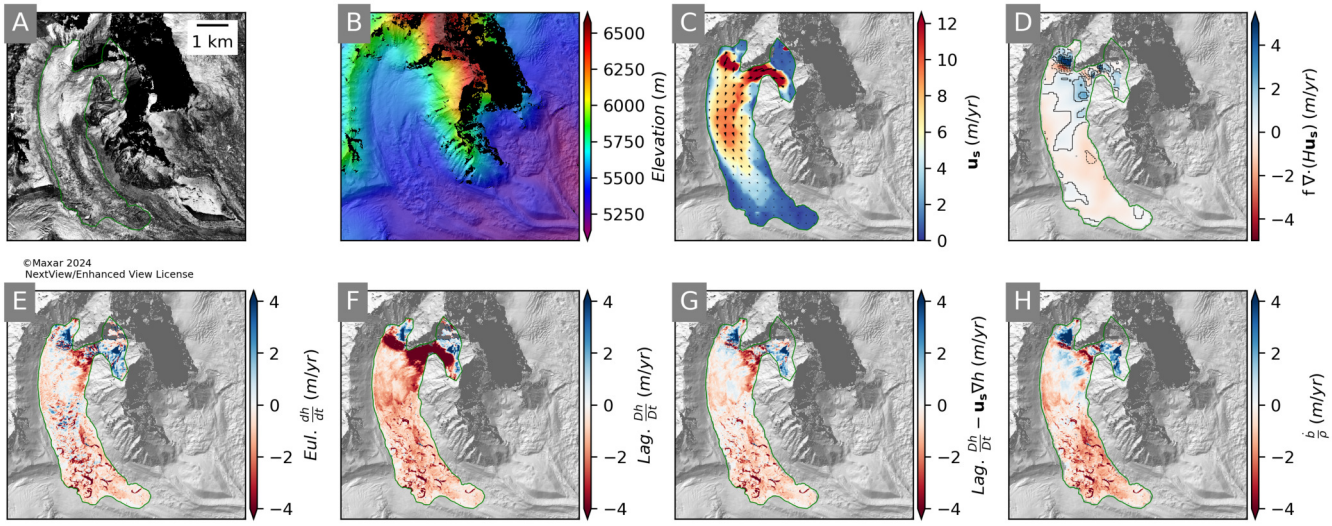

Fig. S3. Subset of data products over Black Changri Nup Glacier for the period 2 November 2015 to 25 October 2016: A) Panchromatic WV03 orthoimage from 2 November 2015. See Figure S2 caption for details.

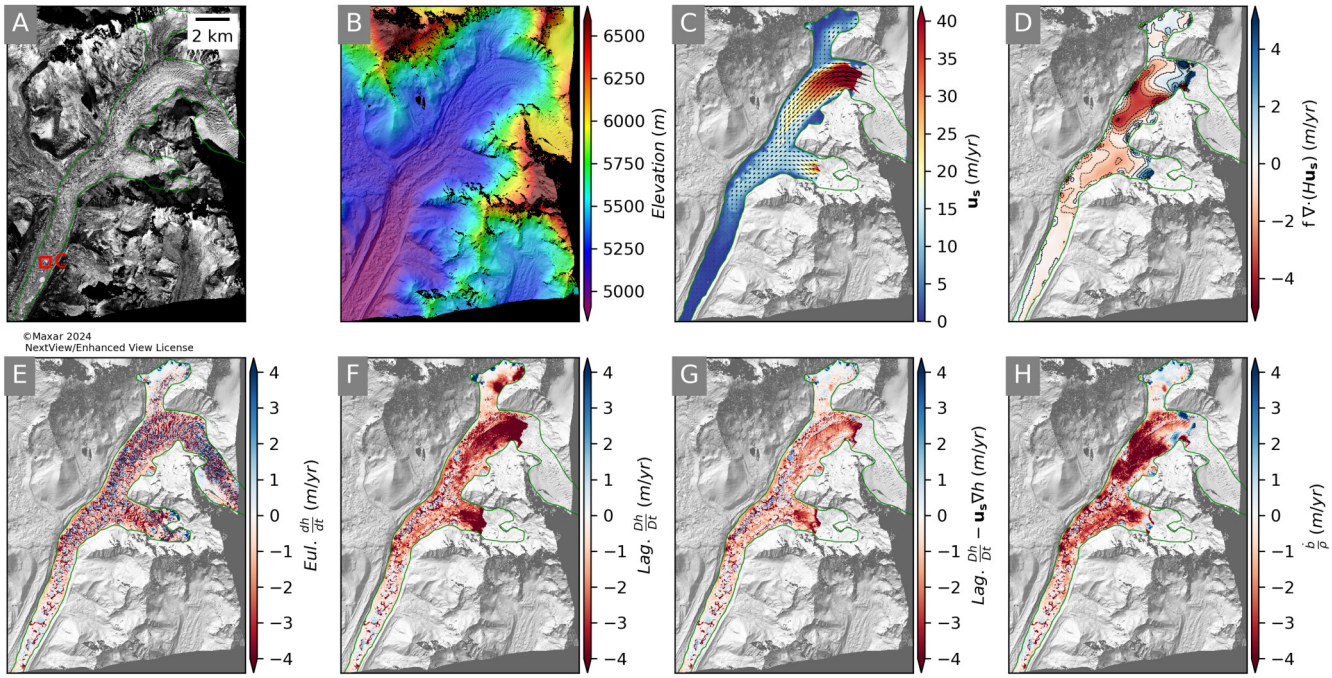

Fig. S4. Subset of data products over Khumbu Glacier for the period 2 November 2015 to 25 October 25 2016: A) Panchromatic WV03 orthoimage from 2 November 2015. See Figure S2 caption for details.

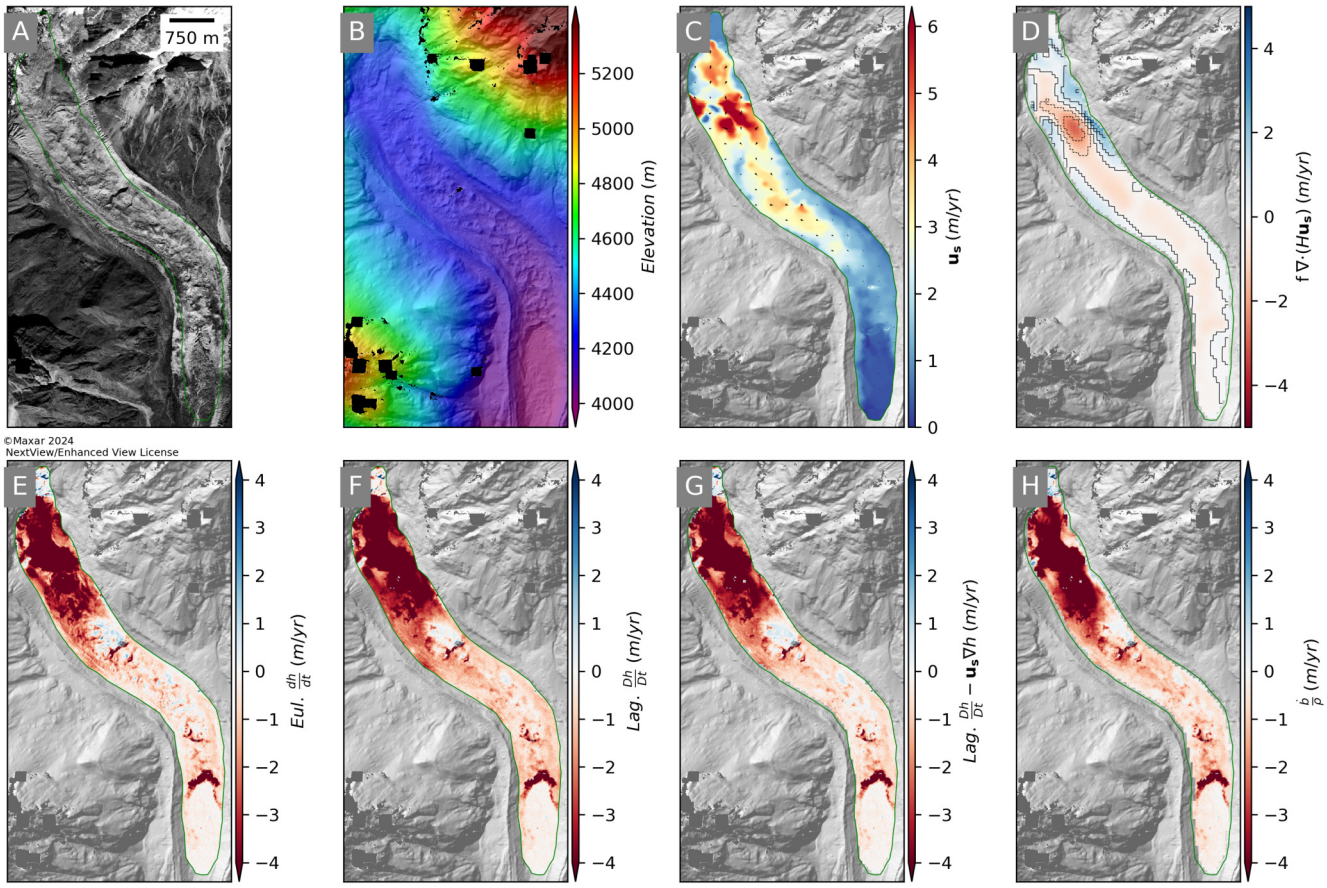

Fig. S5. Subset of data products over Lirung Glacier for the period 6 November 2016 to 22 December 2017: A) Panchromatic WV02 orthoimage from 6 November 2016. See Figure S2 caption for details.

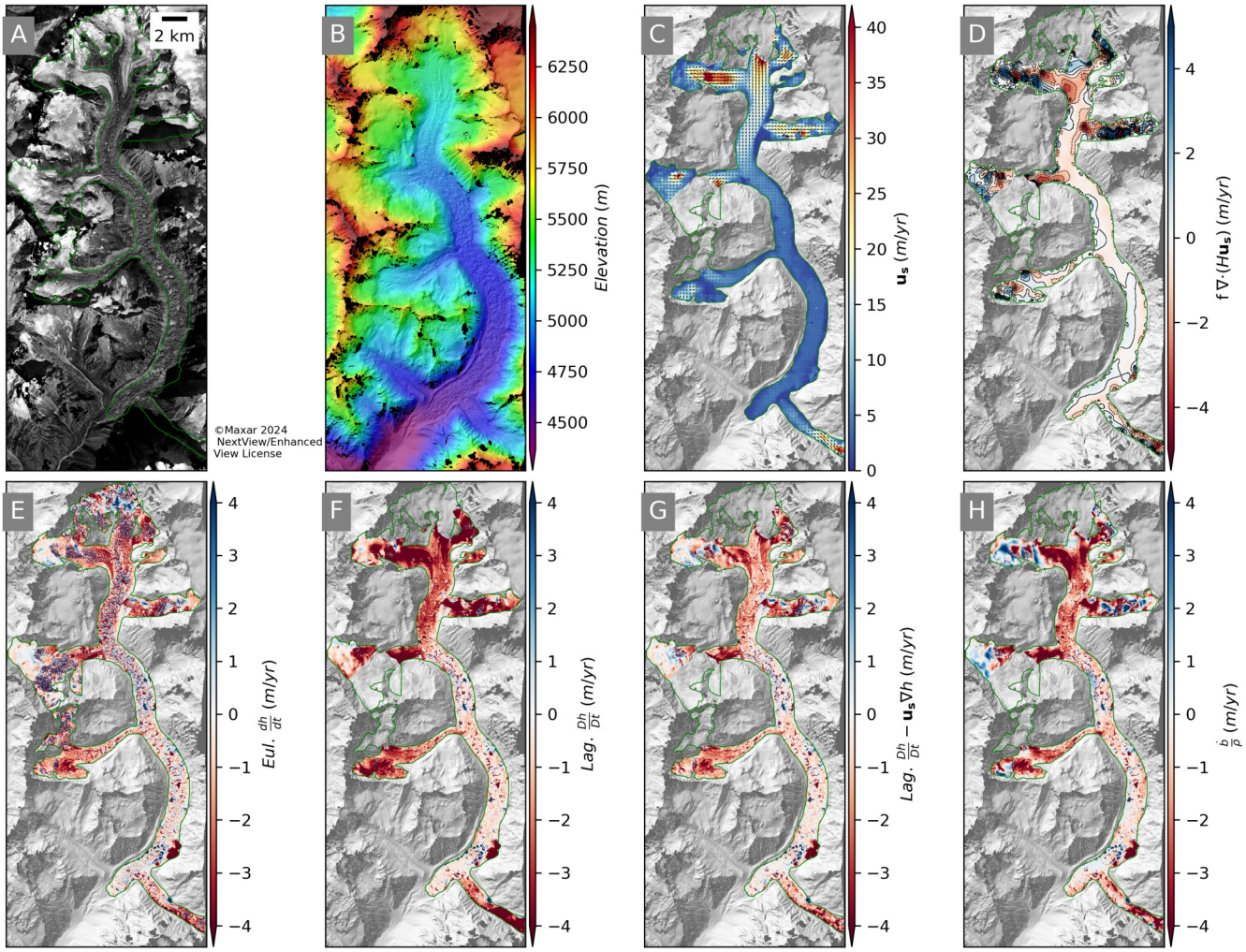

Fig. S6. Subset of data products over Langtang Glacier for the period 22 February 2015 to 7 January 2016: A) Panchromatic WV02 orthoimage from 7 January 2016. See Figure S2 caption for details.

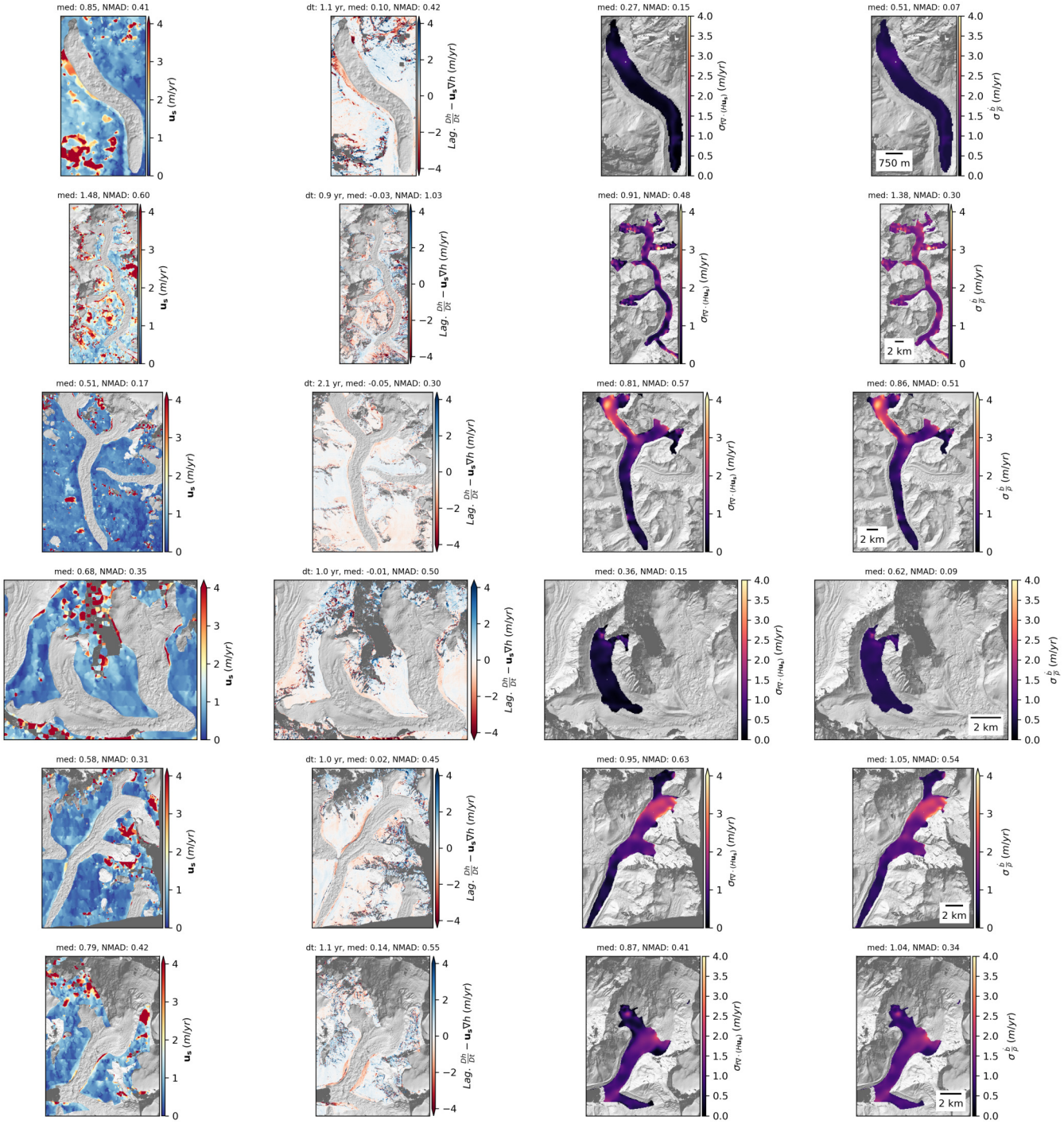

Fig. S7. Components used to derive final Lagrangian SMB uncertainty estimates for the six study glaciers. From left to right, surface velocity ($\boldsymbol{u_s}$) and slope-corrected Lagrangian elevation change rate ($\frac{Dh}{Dt} - \boldsymbol{u_s}\nabla h$) over non-glacierized surfaces assumed to have no change, flux divergence uncertainty (See Section 4.3, Equation 8), the final combined Lagrangian SMB uncertainty ($\sigma_{\frac{\dot{b}}{\rho}}$) from Equation 6. Note that some coherent residuals in the $\frac{Dh}{Dt} - \boldsymbol{u_s}\nabla h$ products are associated with real elevation change signals over moraines, hillslopes, lakes, and seasonal snow.

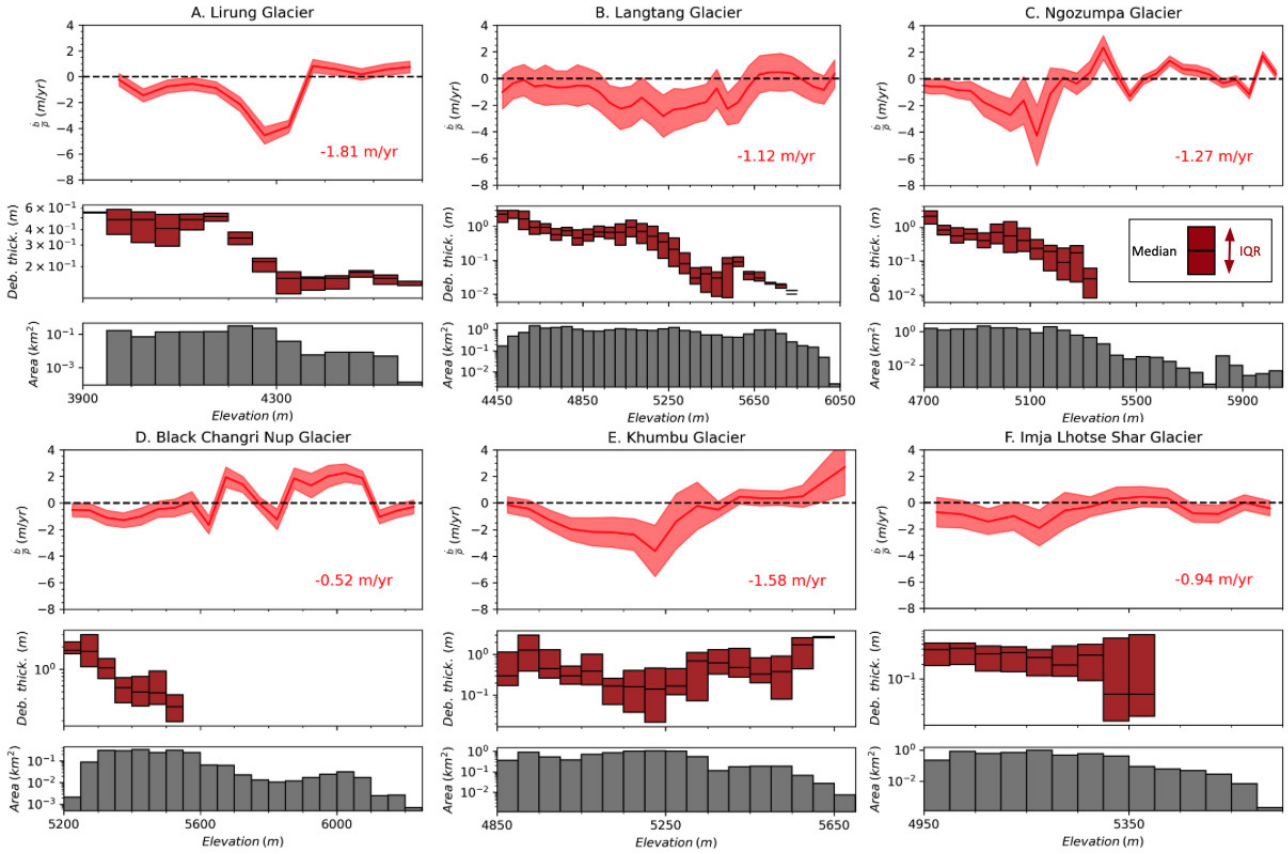

Fig. S8. Same as in Figure 6, but with debris thickness and hypsometry of valid pixels in the Lagrangian SMB rate products plotted on a logarithmic scale.

REFERENCES

Farinotti D, Huss M, Fürst JJ, Landmann J, Machguth H, Maussion F and Pandit A (2019) A consensus estimate for the ice thickness distribution of all glaciers on Earth. *Nature Geoscience*, **12**(3), 168–173, ISSN 1752-0894, 1752-0908 (doi: 10.1038/s41561-019-0300-3)

Frey H, Machguth H, Huss M, Huggel C, Bajracharya S, Bolch T, Kulkarni A, Linsbauer A, Salzmann N and Stoffel M (2014) Estimating the volume of glaciers in the Himalayan–Karakoram region using different methods. *The Cryosphere*, **8**(6), 2313–2333, ISSN 1994-0424 (doi: 10.5194/tc-8-2313-2014)

Fürst JJ, Gillet-Chaulet F, Benham TJ, Dowdeswell JA, Grabiec M, Navarro F, Pettersson R, Moholdt G, Nuth C, Sass B, Aas K, Fettweis X, Lang C, Seehaus T and Braun M (2017) Application of a two-step approach for mapping ice thickness to various glacier types on Svalbard. *The Cryosphere*, **11**(5), 2003–2032, ISSN 1994-0424 (doi: 10.5194/tc-11-2003-2017)

Huss M and Farinotti D (2012) Distributed ice thickness and volume of all glaciers around the globe: GLOBAL GLACIER ICE THICKNESS AND VOLUME. *Journal of Geophysical Research: Earth Surface*, **117**(F4), n/a–n/a, ISSN 01480227 (doi: 10.1029/2012JF002523)

Maussion F, Butenko A, Champollion N, Dusch M, Eis J, Fourteau K, Gregor P, Jarosch AH, Landmann J, Oesterle F, Recinos B, Rothenpieler T, Vlug A, Wild CT and Marzeion B (2019) The Open Global Glacier Model (OGGM) v1.1. *Geoscientific Model Development*, **12**(3), 909–931, ISSN 1991-9603 (doi: 10.5194/gmd-12-909-2019)